42nd AIAA Aerospace Sciences Meeting and Exhibit
5 - 8 January 2004, Reno, Nevada

42nd AIAA Aerospace Sciences Meeting and Exhibit, Reno, Nevada, 5-8 January 2004

DNS OF ATTACHMENT-LINE/CROSSFLOW BOUNDARY LAYER INSTABILITY IN SUPERSONIC SWEPT WING FLOWS

Steven E. Speer* and Xiaolin Zhong†
University of California Los Angeles, Los Angeles, California 90095

Leslie Gong‡ and Robert Quinn§
NASA Dryden, Edwards, California 93523

ABSTRACT

A high-order shock-fitting, finite-difference, direct-numerical-simulation (DNS) Navier-Stokes computer code has been under development. The code has been developed specifically as a tool for investigating the attachment-line and crossflow boundary layer transition mechanisms associated with supersonic/ hypersonic airflows past swept/tapered wing geometries. This paper briefly introduces the importance of studying the fundamental attachment-line and crossflow vortice swept-wing boundary layer instabilities mechanisms and discusses the reasons for approaching the problem using DNS simulations. Preliminary results from several DNS simulations of Mach 5.1 airflow about various parabolic cross-section wing leading edge geometries, differing in leading edge sweep angle and wing taper ratio, will be shown. Also to be shown are initial results from unsteady receptivity simulations where the mean flow solution is excited by a standing acoustic or vorticity wave introduced in the freestream ahead of the bow shock created in front of a swept parabolic leading edge in supersonic flow.

GENERAL INTRODUCTION

For the supersonic/ hypersonic air-vehicle designer being able to predict accurately using analytical or computational methods the laminar-turbulent boundary layer (B.L.) transition locations about practical 3-D geometries is extremely desirable. Skin friction drag and surface heating rates are two important parameters which need to be predicted accurately, the first for range performance considerations and the second to insure vehicle safety by designing an appropriate thermal protection system capable of handling the intense surface heating, which yet will be light enough not to impact the vehicles usable payload very much. Both the skin friction and the surface heating rates are dependent on the type of boundary layer near the vehicles surface. A laminar boundary layer produces less skin friction and lower surface heating rates than a turbulent boundary layer.

Because of these differences it is desirable to know with confidence during the design process where the high-temperature and high drag regions are as a result of boundary layer transition, so that they can be accounted for or alleviated appropriately before the vehicle is made. The designer ultimately would like to be able to make the predictions for any given vehicle geometry without going to the wind tunnel, since wind tunnel models and testing can be expensive. However, currently no such high fidelity practical boundary layer transition prediction method exists.

It is generally recognized that boundary layer transition prediction and control has been an elusive goal for the fluid dynamics community for many years now. This is mainly the result of insufficient understanding of the transition process. The details of the transition process are still not fully understood. In practice many competing instability mechanisms interact nonlinearly

* Ph.D. Student, Mechanical and Aerospace Engineering Department, Member AIAA, speer@seas.ucla.edu
† Professor, Mechanical and Aerospace Engineering Department. Associate Fellow AIAA, xiaolin@seas.ucla.edu
‡ Aerospace Engineer, Aerostructures Branch.
§ Research Scientist, Engineering and Technical Services at NASA Dryden Research Center, 107 Research Drive.

on general 3-D bodies, making it difficult to develop general analytical or computational tools in order to assist the designer to make B.L. transition predictions on practical vehicle geometries. Designing high-speed vehicles with low skin friction drag and efficient thermal protection systems is an iterative process that requires the determination of the B.L. transition locations for many different designs. Wind tunnel experiments can be conducted to assist in the iterative design process, but they are expensive and time consuming to conduct. To keep costs down and speed the design process, efforts have been made over the years to develop analytical and computational techniques to aid in the transition prediction process. It should not be construed that there are no techniques, nor approximate methods to get around the problem. For indeed engineers have solved the problem as evidenced by the flying of many high-speed vehicles (i.e.: SR-71, X-15, Space Shuttle).

The simplest and most conservative method to approaching a boundary layer problem is to simply analyze the flow as if the boundary layer is always turbulent. But if more fidelity is required, one could always assume a transition location and proceed with the analysis, treating the laminar and turbulent regions appropriately. But the problem comes down to knowing where to place this transition position. Multiple methods are currently available for approximating the transition location (i.e. local Reynolds/Mach number conditions, e^N, linear/nonlinear PSE). These methods are based on empirical correlations or analytical methods derived from studying simplified geometries, (i.e. flat plates, cones, rotating disks, etc).

Studying simplified geometries allows researchers to study specific transition mechanisms individually instead of simultaneously as would be necessary for general practical vehicle shapes. After making simplifying assumptions, the mathematical formulations are simpler, hence easier to analyze. Some simplifications that are made along the way in formulating many of the currently available boundary layer transition prediction methods include: neglecting to account for the freestream turbulence levels; assuming parallel flow; and neglecting streamline curvature effects.

The transition prediction methods derived using these simplified geometries make reasonably accurate prediction for geometries not significantly different from those for which the models were derived, but the extension of these methods to more realistic bodies remains nontrivial and so the designer is driven back to the wind tunnel and a new set of experiments. Establishing a database of transition prediction correlations for more general bodies based on such physical experiments is one approach to addressing the transition prediction problem. This approach can be expensive and still will not provide a general understanding of the problem.

Another draw back to studying transition phenomena purely from an experimental approach is the lack resolution and the inability to measure the details of the flow properties in regions of interest. This is a direct result of the boundary layers being so thin. Some common experimental limitations are: the insertion of test probes in the flow will interact and changes the flow field itself; the number of locations where flow properties can be measured are physically limited by the size of the test probes available; or especially relevant to high speed flows, is that the physical environment is simply difficult to reproduce in the laboratory (Mach number too high, flow too hot, flow Reynolds Number can not be matched without adjusting the type of gas used, or playing tricks with temperature and pressure, etc).

One approach available today, which does not suffer from the physical limitations common of experimental approaches nor the requirement to simplify the problem so drastically as is common in analytical formulations, is the use of Direct-Numerical-Simulation (DNS) techniques and the powerful computer systems available today. Using the DNS approach, the most general set of the Navier-Stokes equations can be solved. There is no need to linearize the problem or simply the geometry being analyzed, though this is still done often in order to run simulations whose results can

be compared to those obtained from analytical methods. The most general non-linear phenomena can be studied directly. The properties of the flow field of interest can be resolved by millions of points as opposed to a handful up to several hundred typical of experiments. DNS experiments can be run and the flow properties analyzed, in much more detail than a physical experiment, for flight conditions sometimes too difficult or expensive to study in wind tunnels.

Though there are limitations to numerical techniques be it arising from questions concerning the physical correctness of imposed boundary conditions, to dealing with the finite mathematics of the of the problem, to limitations of computer speed and memory, numerical experiments allow for much deeper analysis of the transition mechanism process or any flow problems in question. Using the powerful techniques of Fourier analysis, one can analyze in detail the propagation and growth of disturbances in a flow at levels only dreamed of by experimentalist. But it should be recognized that DNS only represents a powerful tool that compliments experiments. Both experiments and DNS are required to advance our understanding. Experiments to establish what is realistic and to identify important unexplained phenomena that need further analysis and DNS to delve into the finer aspects of the physics and reproduce the experimental results as validation of successful understanding and implementation.

So to bring this introduction to a close, boundary layer transition prediction is an important unresolved problem in the field of fluid dynamics. For efficient high speed vehicle designs where the vehicle will be required to travel at high speeds for extended periods of time, its is critical to be able to predict where boundary layer transition will occur at a given flight condition. Given that most high speed aerospace vehicles employee slender bodies with swept leading edge wing configurations, or simply blended wing-body concepts with swept leading edges, as a means to reduce shock drag, stagnation temperatures and other adverse phenomena, it is clear from a practical point of view, that understanding the boundary layer transition process on swept wing geometries is of real importance. Fortunate for us, this geometry as far as geometries go is relatively simple. However the simplicity of the geometry should not fool you, for the analysis of boundary layer transition on such a simple geometry is quite complicated and intriguing. Furthermore, despite much research into swept wing transition at subsonic speeds, not much work has been published studying the transition mechanisms at supersonic/hypersonic speeds. Much of the transition studies published for this flight regime are for flat plate, parabolic leading edge, cone, or corner flow geometries.

So since there still exists a knowledge gap in understanding the phenomena of boundary layer transition and for methods to predict where transition will occur, especially for the case of practical supersonic swept wing flows, this paper represents the first of many that this author hopes to contribute as my knowledge and research in to this area grows. This problem will be studied using the Direct-Numerical-Simulation (DNS) code that has been under development over the past couple of years. This paper will briefly describe: the two major transition mechanisms present in swept wing flow, they being the attachment-line and crossflow instabilities, which will be the focus of future detailed analysis. The main features of the DNS code that has been developed and finally some initial numerical results obtained from both steady and unsteady simulations will also be shown.

MAJOR BOUNDARY LAYER TRANSITION MECHANISMS

When studying the literature concerning boundary layer transition, there are 3 major stages in the transition process: 1) Receptivity, 2) Linear growth/ amplification and 3) Secondary instability and nonlinear interactions/breakdown.

The process of receptivity has to do with how various disturbances in the flow outside the boundary layer, be they acoustic waves, entropy waves, or vorticity waves, interact, propagate and change as they enter into the boundary layer. For the case of supersonic/ hypersonic flows, the receptivity process is significantly altered, as

a result of the bow shock that forms ahead and away from the body. In supersonic receptivity one must also be concerned with how the disturbances in the freestream ahead of the shock are processed when passing through the shockwave before entering the boundary layer. For the supersonic swept wing flows to be studied by this author, this will be important.

The linear growth and amplification refers to the way the disturbances present grow or decay in amplitude as they continue to propagate. In the early stages of interaction when the disturbance amplitudes are small the interactions are linear. But as the interaction continues, depending on frequency of the disturbance and on the flow conditions, the amplitudes of the disturbances will either grow (become amplified), stay unchanged, or diminish/ decay. If the interaction is such that the disturbance amplitude grows to have sufficient magnitude then the interactions becomes nonlinear resulting in the third phase of transition.

TRANSITION MECHANISMS SPECIFIC TO SWEPT WING FLOWS

According to the published literature, transition on swept wings involves one or more of the following mechanisms: 1) Attachment-line instabilities or contamination;, 2) Crossflow vortices, either stationary or traveling; 3) Streamwise instabilities, like the common Tollmien-Schlichting (T-S waves); and finally 4) Görtler (centrigual) instabilities.

The attachment-line instability or contamination refers to the disturbances that interact with the flow at the leading edge stagnation line of the swept wing. Figure 1 shows this schematically. These disturbances can be caused by: roughness along the leading edge; the result of the interaction of a fuselage boundary layer with the wing leading boundary layer at the wing-fuselage junction; or as a result of a freestream disturbance being received into the boundary layer at the stagnation attachment-line. This particular instability is of importance to this researcher since this instability can result in transition at the leading edge, thereby ruining the possibility of laminar flow over the remaining portion of the wing. This type of boundary layer transition has been observed on the X-15 and the Space Shuttle.

The second type of instability mechanism deals with the instability of the co-rotating vortices that are produced on swept wings, which are given the name cross-flow vortices. These vortices are produce as a result of the pressure gradients present near the leading edge and in the spanwise direction along the wing. These pressure gradients cause the low momentum flow inside the boundary layer to change direction more than the flow outside the boundary layer. This phenomena produces the characteristic twisting boundary layer profile associated with 3D swept wing flows, but also induces the formation of the crossflow vortices. See figure 1 for a schematic of the crossflow velocity profile. These vortices can either be stationary in nature or can travel. Instabilities in these vortices are the second major contributor to boundary layer transition. Since the phenomena starts in the region near the leading edge, this mechanism is also important to this author.

The last two transitions are not of as much interest to the present study since they tend to occur further down stream on the wing away from the leading edge.

CODE - GOVERNING EQUATIONS

With the proceeding background introducing the swept wing boundary layer behind us, the remainder of this paper will focus on the direct numerical simulation (DNS) code that has been developed specifically to study the instability of attachment-line flow and crossflow vortices near the leading edge of a wing.

The governing equations for the DNS of supersonic/ hypersonic boundary layer transition are the three-dimensional Navier-Stokes equations. Written in conservation-law form in Cartesian coordinates the equations have the following form,

$$\frac{\partial \vec{U}}{\partial t} + \frac{\partial \vec{E}_I}{\partial x} + \frac{\partial \vec{F}_I}{\partial y} + \frac{\partial \vec{G}_I}{\partial z} + \frac{\partial \vec{E}_V}{\partial x} + \frac{\partial \vec{F}_V}{\partial y} + \frac{\partial \vec{G}_V}{\partial z} = 0 \quad (1)$$

where $\vec{U}$ is the conserved flow variable vector. $\vec{E}_I$, $\vec{F}_I$, $\vec{G}_I$ are the respective inviscid convective flux term vectors in the x –direction, y-direction, and k-direction. $\vec{E}_V$, $\vec{F}_V$, $\vec{G}_V$ are the respective viscous flux term vectors in the x –direction, y-direction, and k-direction.

$$\vec{U} = \begin{bmatrix} \rho \\ \rho u \\ \rho v \\ \rho w \\ E_t \end{bmatrix} \tag{2}$$

$$\vec{E}_I = \begin{bmatrix} \rho u \\ \rho u^2 + p \\ \rho uv \\ \rho uw \\ (E_t + p)u \end{bmatrix} \tag{3}$$

$$\vec{E}_v = \begin{bmatrix} 0 \\ \tau_{xx} \\ \tau_{xy} \\ \tau_{xz} \\ u\tau_{xx} + v\tau_{xy} + w\tau_{xz} + q_x \end{bmatrix} \tag{4}$$

$$\vec{F}_I = \begin{bmatrix} \rho v \\ \rho uv \\ \rho v^2 + p \\ \rho vw \\ (E_t + p)v \end{bmatrix} \tag{5}$$

$$\vec{F}_V = \begin{bmatrix} 0 \\ \tau_{xy} \\ \tau_{yy} \\ \tau_{yz} \\ u\tau_{xy} + v\tau_{yy} + w\tau_{yz} + q_y \end{bmatrix} \tag{6}$$

$$\vec{G}_I = \begin{bmatrix} \rho w \\ \rho uw \\ \rho vw \\ \rho w^2 + P \\ (E_t + p)w \end{bmatrix} \tag{7}$$

$$\vec{G}_V = \begin{bmatrix} 0 \\ \tau_{xz} \\ \tau_{yz} \\ \tau_{zz} \\ u\tau_{xz} + v\tau_{yz} + w\tau_{zz} + q_z \end{bmatrix} \tag{8}$$

The details of the numerical schemes used for solving this set of equations has already been published. See Refs. [7],[25],[26],[28],[29],[30] for the specific algorithms and equations. Here I will simply describe what the code consists of. Spatial discretization is handled by 3rd, or 5th order explicit upwind finite difference schemes for the inviscid flux terms and corresponding central difference schemes for the viscous flux terms. A Lax-Friedrich flux splitting scheme is used to decompose the inviscid flux into positive and negative wave fields. The time integration is handled using a 1st, 2nd, or 3rd order Runge-Kutta scheme. The governing equations are transformed using the standard curvilinear coordinate transformation technique. A special feature of this code is that it uses a shock-fitting scheme to track the bow shock, and hence the grid is time dependent. The shock boundary condition uses a Rankine-Hugoniot relation across the shock and a characteristic compatibility equation behind it.

NUMERICAL SIMULATION FLOW CONDITIONS, GEOMETRIES, RESULTS

For the numerical simulations to be shown in this paper, the freestream flow conditions were: Mach number = 5.1, pressure = 4550 Pa, density = 0.07306 kg/m^3, and wall temperature = 1000K. These flow conditions correspond to a flight taken by the X-15 aircraft. The basic shape of the physical grid is shown in figure 2. The grid is of the structured body conforming type.

Through out code development the standard grid refinement technique was used, in order to insure that the results obtained were grid independent. That is to say each time the grid was doubled and a comparison was made between the corresponding points of the flow, until the difference between solutions on each grid matched within a specified tolerance.

Initially three grid densities were used for the i- and j-directions, each time doubled, while the type of simulation being tested determined the number of points in the k-direction. The grid sizes were of the type: 1) I = 87, J = 61, K = 1(2-D or pseudo 3-D), 4, 8, 20; 2) I = 167, J = 121, K = 1(2-D or pseudo 3-D), 4, 8, 20; or 3) I = 327, J = 241, K = 1(2.-D or pseudo 3-D), 4, 8, 20. Leading edge sweep angle was one of the following: 0°(no sweep), 20 °, 36.75 °, 45 °. The cross-section profiles of the grid tested were parabolic, where the surface ordinates were given by the following equation, $x = by^2 - d$. The taper ratio of the wing is equal to the ratio of tip chord to root chord (see figure 2). Initial simulations were run with a taper ratio = 1, which corresponds to a purely swept wing.

Later once the swept taper geometry was correctly implemented in the code, a test matrix of means flows were ran to form a foundation of solutions from which later unsteady receptivity solutions could be run. The test matrix of mean flow solutions is shown in table 1. A representative sample of three different mean flow solutions is shown in figures 3. They correspond to a 50% taper wing with 30, 45, and 60 degrees of sweep, respectively. These mean flows were ran long enough such that the relative error between corresponding grid points after 100,000 iterations were 10^{-10}. This high level of convergence is required so that when the receptivity simulations are ran, using small 1-2% magnitude perturbation disturbances, the Fourier analysis will see the imposed disturbances and not numerical noise from and insufficiently converged mean flows.

Another metric that was used to judge solution convergence at a given time-step, was the L2 norm of the non-dimensional time-derivative of each conserved variable, obtained before the time integration is computed for the next iteration. Time history plots of the mean, maximum and minimum residuals were viewed to judge convergence. The residual for a mean flow solution should approach the machine zero of the computer. The computations here are computed using double precision, thus the residual should be approach magnitudes on the order of 10^{-15} or so when fully converged. Figure 4 shows representative time history residual plots for a mean flow and a for an unsteady receptivity problem excited by a freestream acoustic wave. Here the mean flow residual is seen to be around 10^{-14}. Figure 5 shows the pressure contour plot of the mean flow solution corresponding to this level of convergence. Figures 6 and 7 show the variation of the u-velocity and the w-velocity components in the direction normal to the surface at several downstream locations beginning first at the leading edge. The boundary layer velocity profiles can be clearly seen.

With confidence in the ability to compute mean flow solutions, unsteady recepticity simulations were begun. Initially acoustics waves were used to excite the flow because they were compatible with a symmetry boundary condition that was used at the leading edge of the wing. The symmetry condition was used in order to allow the computation of only half the flow field around the wing leading edge during mean flow computations. This works fines. Figure 8 shows the instantaneous perturbation pressure (the current solution minus the mean flow solution) contours, for two different acoustic wave angles, 0 degree and 22.5 degree relative to the freestream flow direction. Line plots in Figure 9 show the variation of the instantaneous pressure perturbation along the surface of the body at four different spanwise locations for the 0 degree acoustic wave case. Note due to the periodic oscillation imposed by the acoustic wave, the convergence residual maintains a small constant value after a periodic state is obtained. See Figure 4. For definition of disturbance types and angle nomenclature see reference paper [7].

But when receptivity analysis due to freestream vorticity waves was required because vorticity waves

are the disturbance type that excites the cross flow vortex instabilities most, this required the removal of the symmetry condition. Now instead the entire domain around the leading edge needed to be simulated. With this modification it was possible to run receptivity simulations excited by a freestream vorticity wave. Figure 10 shows the initial simulation results for a 0 deg vorticity wave. The plots show the instantaneous perturbation pressure and density contour plots. Again the perturbation quantity is obtained by subtracting the mean flow away from the actual solution with the unsteady wave imposed.

Due to late completion of the computer code, detailed analysis of the flow receptivity problem could not be completed and included in this paper. Those results will have to wait until the next paper.

FUTURE WORK

With preliminary completion of the main DNS simulation computer code, focus can now be placed on developing the Fourier analysis tools required to analysis the simulations in more detail. Fourier coefficients and phase angles are initially what are desired so that the detailed information about the disturbances can be extracted from the computed flow field. Later detailed computation of disturbance growth rates will be required as well as comparisons to linear stability theory.

SUMMARY

A high-order shock-fitting finite-difference direct-numerical-simulation (DNS) Navier-Stokes computer code has been developed specifically to study the two main swept wing boundary layer transition mechanisms –attachment-line and crossflow instabilities. Some introductory background information pertinent to these topics has been discussed and preliminary qualitative validation of the computer code has been completed. Some representative results from several initial simulations have been presented.

ACKNOWLEDGEMENTS

This work was sponsored by NASA Dryden Flight Test Center, Edwards CA and was monitored by Les Gong and Robert Quinn.

REFERENCES

[1] Cebeci, Tuncer; and Chen, Hsun H.: Numerical Method for Predicting Transition in Three-Dimensional Flows by Spatial Amplification Theory. AIAA Journal. Vol. 30, No. 8, August 1992.

[2] Coleman, Colin P.; Poll, D. I. A.; Laub, James A.; and Wolf, Stephen W. D.: Leading Edge Transition on a 76-Degree Swept Cylinder at Mach 1.6. AIAA 96-2082. June 17-20, 1996. New Orleans, LA.

[3] Coleman, Colin P.; Poll, D. I. A.; and Lin, Ray-Sing: Experimental and Computational Investigation of Leading Edge Transition at Mach 1.6. AIAA 97-1776. Jun 29-July 2, 1997. Snowmass Village, CO.

[4] Collis, S. Scott: A Computational Investigation of Receptivity in High-Speed Flow near a Swept Leading-Edge. Ph.D. Dissertation. Department of Mechanical Engineering. Stanford University. March 1997.

[5] Collis, Scott; and Lele, Sanjiva K.L: A Computational Approach to Swept Leading-Edge Receptivity. AIAA Aerospace Science Conference, AIAA-96-0180. Reno NV.

[6] Creel, T. R. Jr.; Beckwith, I. E.; and Chen, F. J.: Transition on Swept Leading Edges at Mach 3.5. Journal of Aircraft. Vol. 24, No. 10. October 1987.

[7] Dong, Haibo; and Zhong, Xiaolin: Numerical Simulations of Transient Growth in a Mach 15 Boundary Layer over a Blunt Leading Edge. AIAA 2003-1226. January 6-9, 2003. Reno, NV.

[8] Gaster, M.: On the Flow along Swept Leading Edges. The Aeronautical Quarterly. V18. May 1967.

[9] Jeyasingham, Samarasingham: Stability of Three-Dimensional Compressible Boundary-Layers. Master of Science Thesis. Aerospace Engineering. Old Dominion University. May 1999.

[10] Joslin, Ronald D.: Direct Simulation of Evolution and Control of Three-Dimensional Instabilities in Attachment-Line Boundary Layers. Journal of Fluid Mechanics (1995), Vol. 291, pp. 369-392.

[11] Kawakami, M.; Kohama, Y.; and Okutsu, M.: Stability Characteristics of Stationary Crossflow Vortices in Three-Dimensional Boundary Layer. AIAA 99-0811. January 11-14, 1999. Reno NV.

[12] Lin, Ray-Sing; and Malik, Mujeeb R.: On the Stability of Attachment-line Boundary Layers. Part 1. The Incompressible Heimenz flow. Journal of Fluid Mechanics (1996) Vol. 311, pp. 239-255.

[13] Lin, Ray-Sing; and Malik, Mujeeb, R.: On the stability of Attachment-line Boundary Layers. Part

2. The Effect of Leading-edge Curvature. Journal of Fluid Mechanics (1997) Vol. 333, pp. 125-137.
[14] Mack, Leslie M.: Boundary-Layer Linear Stability Theory. Annual Review of Fluid Mechanics. March 1984.
[15] Mack, Leslie M.: On the Stability of the Boundary Layer on a Transonic Swept Wing. AIAA 1979.
[16] Malik, M. R.: Numerical Methods for Hypersonic Boundary Layer Stability. Journal of Computational Physics, 86, 376-413 (1990).
[17] Malik, Mujeeb R.; and Beckwith, Ivan E.: Stability of a Supersonic Boundary Layer along a Swept Leading Edge. AGARD-CP-438. October 1988.
[18] Murakami, A.; Stanewsky, E.; and Krogmann, P.: Boundary Layer Transition on Swept Cylinders at Hypersonic Speeds. AIAA 95-2276. June 19-22, 1995. San Diego, CA.
[19] Nomura, Toshiyuki: Stability Analysis of Supersonic Swept-Wing Bondary Layers. AIAA 2003-4145. June 23-26, 2003. Orlando, Floida.
[20] Poll, D. I. A.: Leading Edge Transition on Swept-Wings. AGARD publication. No. 21. 1967.
[21] Poll, D. I. A.: Transition in the Infinite Swept Attachment Line Boundary Layer. The Aeronautical Quarterly, Vol. XXX, pp. 607-629, November 1979.
[22] Reibert, M. S.; and Saric, W. S.: Review of Swept-wing Transition. AIAA 97-1816. June 29-July2, 1997. Snowmass Village, CO.
[23] Saric, S. Saric;, Reed, Helen L.; and White, Edward B.: Stability and Transition of Three-Dimensional Boundary Layers. Annu. Rev. Fluid Mech. 2003. 35:413-40.
[24] Wassermann, Peter; and Kloker Marku: Transition Mechanisms Induced by Travelling Crossflow Vortices in a Three_Dimensional Boundary Layer. J. Fluid Mech. (2003) Vol. 483, pp. 67-89.
[25] Whang, Chong W.; and Zhong, Xiaolin: Leading Edge Receptivity of Görtler Vortices in a Mach 15 Flow over a Blunt Wedge. AIAA 2003-0790, January 6-9, 2003. Reno NV.
[26] Whang, Chong W.; and Zhong, Xiaolin: Receptivity of Görtler Vortices in Hypersonic Boundary Layers. AIAA 2002-0151, January 14-17, 2002. Reno NV.
[27] White, E. B.; and Saric, W. S.; and Gladden, R. D.; and Gabet, P. M.: Stages of Swept Wing Transition. AIAA 2001-0271. January 8-11, 2001. Reno NV.
[28] Zhong, Xiaolin: High-Order Finite-Difference Schemes for Numerical Simulation of Hypersonic Boundary-Layer Transition. Journal of Computational Physics. Vol. 144, 662-709, (1998).
[29] Zhong, Xiaolin: Additive Semi-Implicit Runge-Kutta Schemes for Computing High-Speed Nonequilibrium Reactive Flows, J. Comput. Phys. 128, 19 (1996).
[30] Zhong, Xiaolin. Leading -edge Receptivity to Free-stream Disturbance Waves for Hypersonic Flow Over a Parabola. J. Fluid Mech. (2001), vol. 441,pp.315-367.

TABLES

	Taper Ratio (Tip Chord/Root Chord)			
Sweep Angle	0.25	0.5	0.75	1.0
0				X
30		X		
45	X	X	X	
60		X		

Table 1: Mean flow run matrix showing sweep angle and taper ratios used.

FIGURES

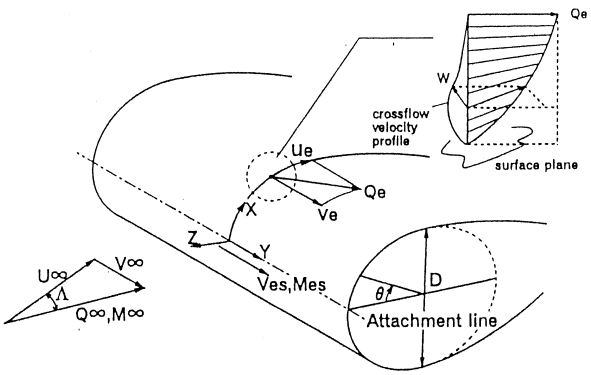

Figure 1: Schematic of attachment-line and cross-flow velocity profile.

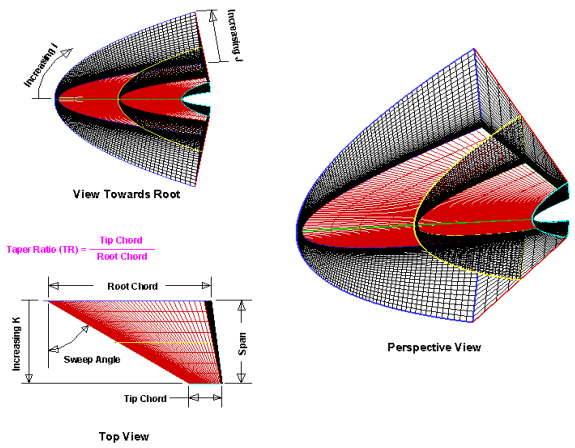

Figure 2: Sample swept/taper parabolic cross-section leading edge grid

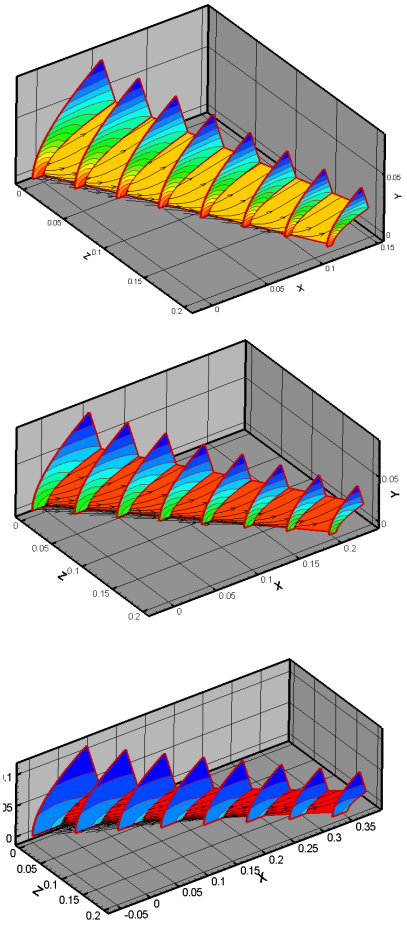

Figure 3: Temperature contours plots for three cases from the mean flow test matrix. Each has a 50% taper ratio. Leading edge sweep angle: 30 degrees (top wing), 45 degrees (middle wing), and 60 degrees (bottom wing). All have a parabolic cross-section leading edge. Test cases run at Mach 5.1.

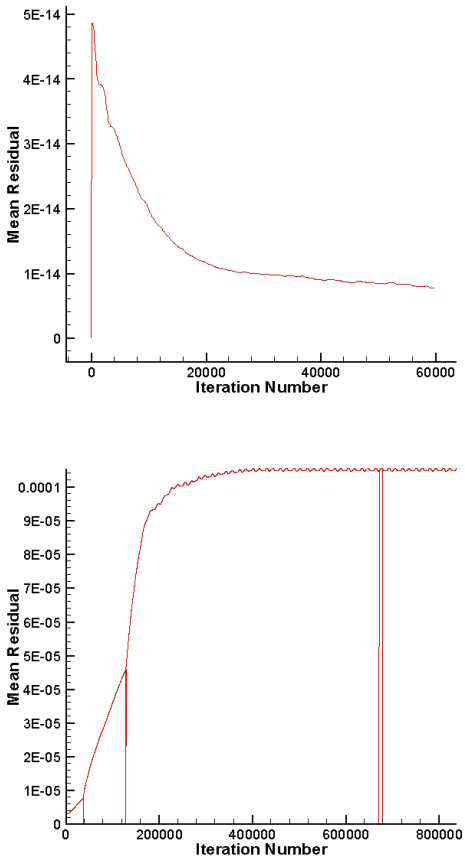

Figure 4: Time history plot of mean residual for mean flow (top) and for an unsteady simulation where the mean flow has been excited by an acoustic wave (bottom). 45 deg. pure sweep, no taper, parabolic cross-section leading edge test cases run at Mach 5.1.

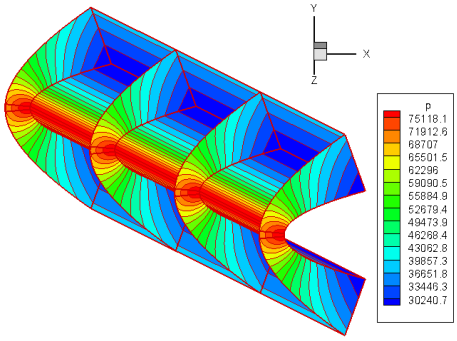

Figure 5: Meanflow pressure contours. 45 deg. pure sweep, no taper, parabolic cross-section leading edge test case run at Mach 5.1.

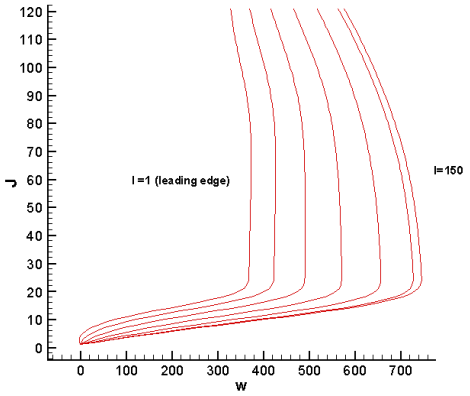

Figure 7: W-velocity boundary layer profiles from 7 positions along the surface, starting at the leading edge and moving downstream. 45 deg. pure sweep, no taper, parabolic cross-section leading edge test case run at Mach 5.1.

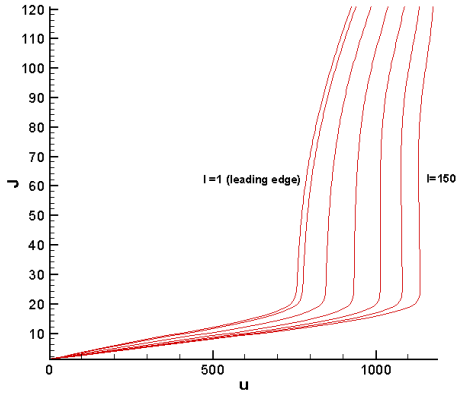

Figure 6: U-velocity boundary layer profiles from 7 positions along the surface, starting at the leading edge and moving downstream. 45 deg. pure sweep, no taper, parabolic cross-section leading edge test case run at Mach 5.1.

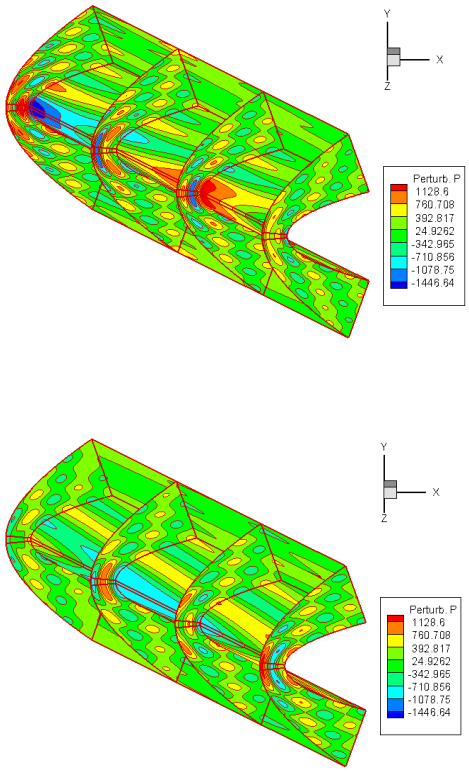

Figure 8: Instantaneous pressure perturbation contours induced by a freestream acoustic wave at 0 deg. relative to flow direction (top) and 22.5 deg relative to flow direction (bottom). Pure sweep, no taper, parabolic cross-section leading edge test cases run at Mach 5.1.

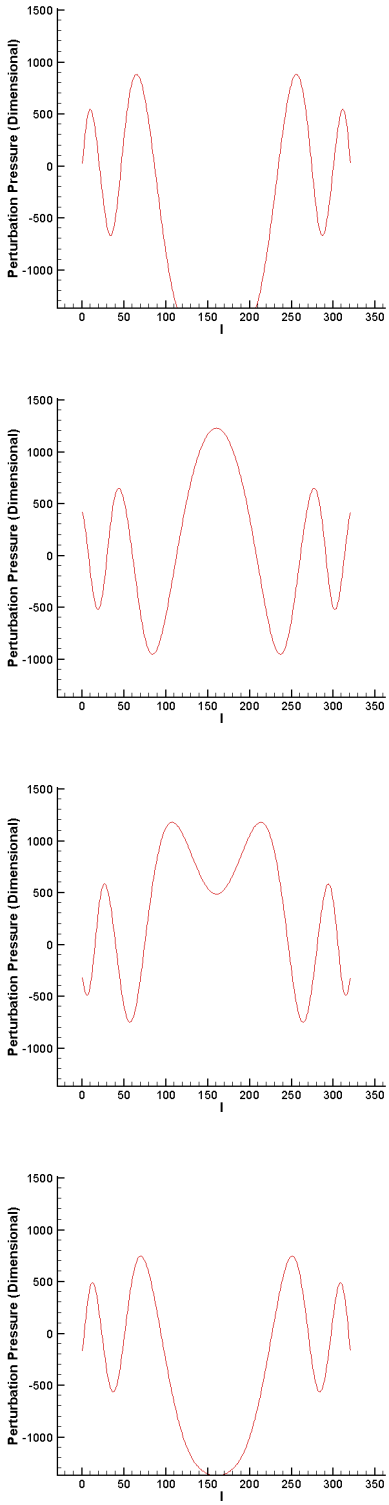

Figure 9: Four instantaneous pressure perturbation variation plots along the surface of the leading edge modeled, induced by a freestream acoustic wave at 0 deg. relative to flow direction. 45 deg. pure sweep, no taper, parabolic cross-section leading edge test case run at Mach 5.1.

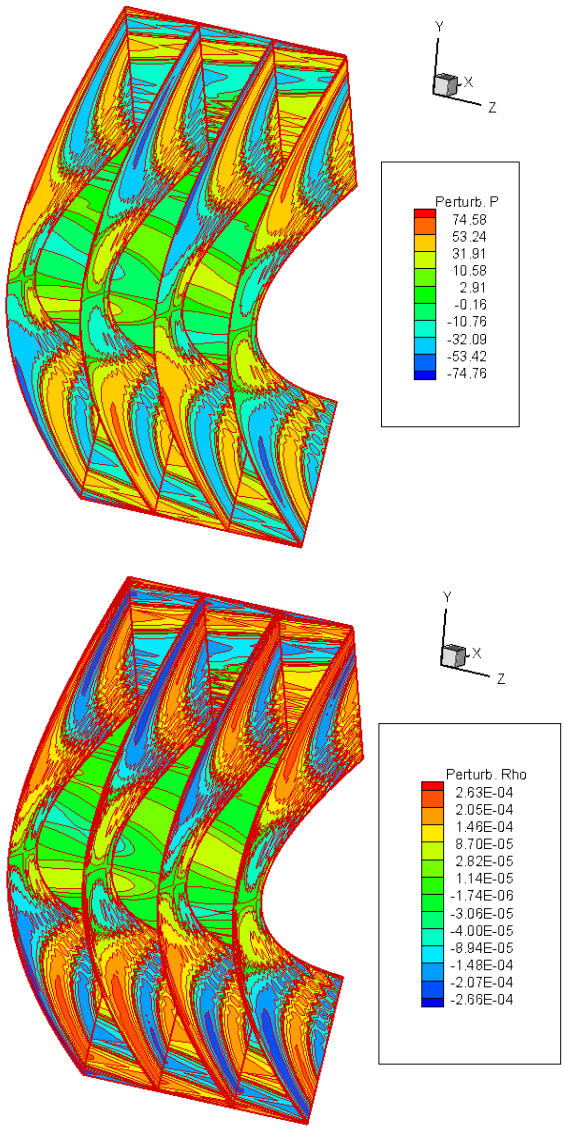

Figure 10: Instantaneous pressure perturbation contours (top) and density perturbation contours (bottom) induced by a freestream vorticity wave (0 deg. relative to flow direction). 45 deg. pure sweep, no taper, parabolic cross-section leading edge test cases run at Mach 5.1.